Aalto University

OPEN ACCESS

This is an electronic reprint of the original article.
This reprint may differ from the original in pagination and typographic detail.

Kettunen, Henrik; Wallén, Henrik; SIhvola, Ari

Tailoring effective media by Mie resonances of radially-anisotropic cylinders

Published in:
Photonics

DOI:
10.3390/photonics2020509

Published: 01/01/2015

Document Version
Publisher's PDF, also known as Version of record

Published under the following license:
CC BY

Please cite the original version:
Kettunen, H., Wallén, H., & SIhvola, A. (2015). Tailoring effective media by Mie resonances of radially-anisotropic cylinders. *Photonics*, *2*(2), 509-526. https://doi.org/10.3390/photonics2020509

This material is protected by copyright and other intellectual property rights, and duplication or sale of all or part of any of the repository collections is not permitted, except that material may be duplicated by you for your research use or educational purposes in electronic or print form. You must obtain permission for any other use. Electronic or print copies may not be offered, whether for sale or otherwise to anyone who is not an authorised user.

Photonics **2015**, *2*, 509-526; doi:10.3390/photonics2020509

OPEN ACCESS

photonics

ISSN 2304-6732

www.mdpi.com/journal/photonics

Article

Tailoring Effective Media by Mie Resonances of Radially-Anisotropic Cylinders

Henrik Kettunen [1,*], Henrik Wallén [2] and Ari Sihvola [2]

[1] Department of Mathematics and Statistics, University of Helsinki, P.O. Box 68, Helsinki FI-00014, Finland

[2] Department of Radio Science and Engineering, School of Electrical Engineering, Aalto University, P.O. Box 13000, FI-00076 Aalto, Finland; E-Mails: henrik.wallen@aalto.fi (H.W.); ari.sihvola@aalto.fi (A.S.)

* Author to whom correspondence should be addressed; E-Mail: henrik.kettunen@helsinki.fi

Received: 18 April 2015 / Accepted: 9 May 2015 / Published: 14 May 2015

Abstract: This paper studies constructing advanced effective materials using arrays of circular radially-anisotropic (RA) cylinders. Homogenization of such cylinders is considered in an electrodynamic case based on Mie scattering theory. The homogenization procedure consists of two steps. First, we present an effectively isotropic model for individual cylinders, and second, we discuss the modeling of a lattice of RA cylinders. Radial anisotropy brings us extra parameters, which makes it possible to adjust the desired effective response for a fixed frequency. The analysis still remains simple enough, enabling a derivation of analytical design equations. The considered applications include generating artificial magnetism using all-dielectric cylinders, which is currently a very sought-after phenomenon in optical frequencies. We also study how negative refraction is achieved using magnetodielectric RA cylinders.

Keywords: radial anisotropy; Mie scattering; artificial magnetism; double-negative media; metamaterials; homogenization

---

1. Introduction

Much theoretical and experimental work has been done in research on advanced artificial electromagnetic metamaterials in recent years [1]. One of the major objectives has been the realization of a negative refractive index, which is required for constructing a perfect lens [2,3]. However, negative refraction does not manifest in naturally-existing materials. Instead, it requires a double-negative (DNG) medium, where both material parameters, permittivity ε and permeability μ, are simultaneously negative. Negative permittivity is observed for some metals at optical and UV frequencies, making them capable of supporting plasmonic waves and resonances. The study of plasmonics [4] has hence been closely related to metamaterials research.

Negative μ is still something that needs to be achieved artificially using, for instance, split-ring resonators (SRR) [5]. However, metallic structures are usually lossy, and as their performance is largely based on geometric details, their response becomes anisotropic, and they are only applicable for a certain polarization and certain angles of incidence. In the visible regime, metals also lose their conductivity and become plasmonic. That is, creating a homogeneous material with negative refraction for visible light requires optical magnetism, which is not naturally available nor realizable using conducting metallic structures.

Therefore, an alternative approach has been to consider all-dielectric metamaterials based on Mie resonances [6–8]. Dielectric materials usually have lower losses, and their dispersion is more moderate in comparison to metals, making the possible applications more broadband. Their analysis is based on Mie scattering theory, which can be analytically applied for 3D spheres and 2D cylinders [9,10]. However, other geometries have been considered, as well. The efforts toward achieving optical magnetism are extensively reviewed in [11], and experimental results have been reported, e.g., for spheres [12] and cubes [13].

Effective materials based on Mie resonances consist of collections of resonant particles. This homogenization procedure was considered for a cubic lattice of spheres by Gans and Happel [14] already in 1909 (In German), and their result was applied for rain drops by Stratton [15] in 1930. However, the paper of Lewin [16] from 1947 is nowadays much better known. Since then, many others have followed this approach [17–26]. Using only isotropic dielectric spheres, the DNG condition is very difficult to achieve. Therefore, different authors have considered, e.g., magnetodielectric spheres [19], spheres of two different sizes [22,23] and layered structures [21,25,26].

Already earlier, magnetic activity and negative permeability were predicted for high-permittivity (ferro)dielectric cylinders [6]. Furthermore, [27–30] apply the Mie theory for circular cylinders, which is also our approach in this paper. Dynamic polarizability tensors of circular cylinders are studied in [31,32], and [33] gives a more general overview on the cylindrical Mie resonances. A more mathematical approach to the homogenization problem is given, e.g., in [34]. Again, achieving the DNG condition using only dielectric cylinders seems challenging. Therefore, [30] suggests a hierarchical approach of using two kinds of cylinders of different size scales. Unlike for spheres, the response of cylinders depends on the polarization. In [27], it is speculated how, by combining both transverse electric (TE) and transverse magnetic (TM) resonances, a DNG region can be achieved using only high-permittivity dielectric rods. However, [35] experimentally shows that the DNG condition can be

achieved for such rods using only TM polarization, where the electric field is parallel to the cylinder axis. On the other hand, [36] reports numerical results that question the validity of this homogenization approach.

Moreover, experimental results for THz-range negative μ have been reported for non-circular dielectric rods [37], and [38] numerically considers optical DNG condition for hybrid stacked rectangular rods.

In this article, we suggest a composite metamaterial, where the inclusions are circular magnetodielectric radially-anisotropic (RA) cylinders. The electrostatic analysis of RA cylinders is considered in [39,40], and the Mie theory is applied for them in [41–43]. Papers [41] and [40] consider using cylindrical RA shells for cloaking purposes, whereas [42,43] focus on the peculiarities of light scattering from plasmonic RA cylinders. For the analysis, occurrence and applications of 3D radially-anisotropic spheres, see [44,45] and the references therein. Mie resonances of anisotropic spheres have also been studied in [46], but the anisotropy is given with respect to rectangular coordinates. Herein, we study how the intrinsic material parameter components affect the Mie resonances of RA cylinders and consider the retrieval of the effective parameters ε_{eff} and μ_{eff} of a homogenized lattice of cylinders.

The homogenization process of RA cylinders builds on different levels, as depicted in Figure 1. As a realization of an RA cylinder, we can consider a structure that consists of either adjacent sectors or concentric layers of two or more materials. If the number or alternating sectors/layers is large enough and the intrinsic details of the cylinder are very small with respect to the wavelength, the cylinder shows different responses in radial and tangential directions. Such structures could then be modeled radially anisotropically with material parameters of dyadic form, $\overline{\overline{\varepsilon}}$ and $\overline{\overline{\mu}}$, whose components are constants in cylindrical coordinates. A similar case of internal homogenization of a layered 3D sphere is studied in [47]. Building on Mie scattering theory, we first model an individual cylinder effectively isotropically, which can also be referred to as internal homogenization (see Figure 1a).

The second level of homogenization is to consider an infinite square lattice of cylinders with lattice constant d, which is further modeled as an effective medium with material parameters ε_{eff} and μ_{eff}, as shown in Figure 1b. The objective of this paper is to show that these effective parameter values can be tailored for a certain frequency by tuning the occurrence of the electric and magnetic Mie resonances of the individual RA cylinders by appropriately choosing the components of the intrinsic dyadics $\overline{\overline{\varepsilon}}$ and $\overline{\overline{\mu}}$. The real virtue of radial anisotropy is that it provides useful extra parameters, but the geometry itself remains canonical. Hence, the scattering analysis for RA cylinders is not significantly more complicated compared with the ordinary isotropic case.

This paper approaches the problem from a theoretical point of view, that is, for instance, considering possible realizations of the suggested structures in Figure 1a with given material parameter values is left out of scope at this stage. We, however, aim to find configurations with material parameter values within a somewhat feasible range. Neither do we consider any specific frequency range, but the results are scalable as far as the unit cell size d can be considered much smaller than the wavelength of impinging fields. The possible applications that we consider include creating and tuning an artificial magnetic response using all-dielectric cylinders, which would prove very useful in the visible range, where natural magnetism is negligible. Another intriguing objective is double-negative (DNG) materials.

In previously-mentioned articles, the DNG effect is usually sought without considering the actual ε_{eff} and μ_{eff} values. Our magnetodielectric RA approach instead aims at being able to tune the desired effective material parameter values at the desired frequency. Especially, our target is to make the effective material parameters satisfy $\varepsilon_{\text{eff}} = \mu_{\text{eff}} = -1$, which gives us negative refractive index $n = -1$, being the well-known condition for the perfect lens [2,3].

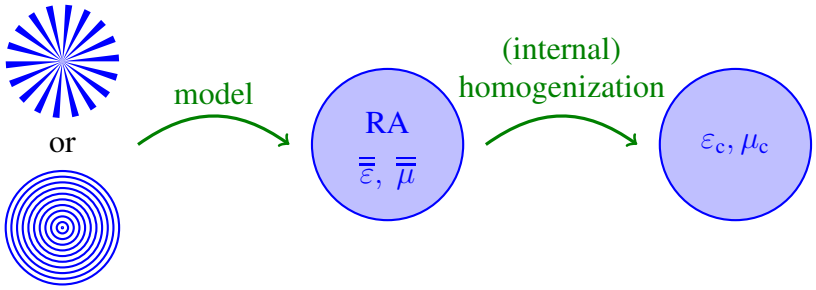

(a) Homogenization of individual cylinders

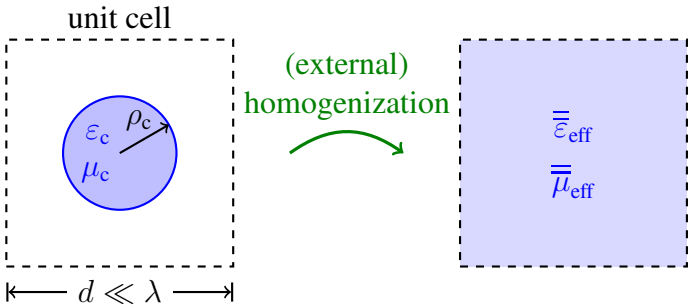

(b) Homogenization of a lattice of cylinders

Figure 1. Schematic illustration of the homogenization procedure. RA, radially-anisotropic.

2. Scattering from an RA Cylinder

The material parameters for a cylindrical RA medium are given in the most general form as:

$$\overline{\overline{\varepsilon}} = \varepsilon_0(\varepsilon_\rho \mathbf{u}_\rho\mathbf{u}_\rho + \varepsilon_\varphi \mathbf{u}_\varphi\mathbf{u}_\varphi + \varepsilon_z \mathbf{u}_z\mathbf{u}_z) \tag{1}$$

$$\overline{\overline{\mu}} = \mu_0(\mu_\rho \mathbf{u}_\rho\mathbf{u}_\rho + \mu_\varphi \mathbf{u}_\varphi\mathbf{u}_\varphi + \mu_z \mathbf{u}_z\mathbf{u}_z) \tag{2}$$

In the following, we study time-harmonic plane wave scattering from a circular RA cylinder using time convention $e^{j\omega t}$. Let the axis of the cylinder be along the z-axis and the incoming wave propagate into the positive x-direction. The cylinder is surrounded by free space with wave number $k_0 = \omega\sqrt{\varepsilon_0\mu_0}$. The full scattering problem is solved as a superposition of two orthogonal polarizations.

For TE$_z$ polarization, the fields of the incoming wave propagating in x-direction are given as:

$$\mathbf{H}_{\text{inc}} = \mathbf{u}_z H_{0z} e^{-jk_0 x} \tag{3}$$

$$\mathbf{E}_{\text{inc}} = \mathbf{u}_y \frac{k_0}{\omega\varepsilon_0} H_{0z} e^{-jk_0 x} \tag{4}$$

Hence, only the material parameter components ε_ρ, ε_φ and μ_z are visible to the impinging wave, and the cylinder can actually be considered magnetically isotropic.

For TM_z polarization, the incoming fields are:

$$\mathbf{E}_{\text{inc}} = \mathbf{u}_z E_{0z} e^{-jk_0 x} \tag{5}$$

$$\mathbf{H}_{\text{inc}} = -\mathbf{u}_y \frac{k_0}{\omega\mu_0} E_{0z} e^{-jk_0 x} \tag{6}$$

and the required material parameters are μ_ρ, μ_φ and ε_z, that is the cylinder seems only magnetically anisotropic.

However, the problem needs to be solved mathematically only once, since due to the duality of electromagnetic fields [48], the orthogonal solution is obtained by substitution:

$$\mathbf{E} \to -\mathbf{H}, \quad \mathbf{H} \to \mathbf{E}, \quad \overline{\overline{\varepsilon}} \leftrightarrow \overline{\overline{\mu}} \tag{7}$$

Therefore, in the following, the analysis and all of the computational results are presented only for the TE_z polarization. This can be seen as a continuation from our previous RA studies [40,45], where permittivity $\overline{\overline{\varepsilon}}$ is always assumed anisotropic. Even though our analysis remains purely theoretical and speculative considering the actual realization of the suggested material configurations, depending on the frequency range, physically-available materials usually offer a wider variety of realizable values for permittivity than for permeability, which also supports choosing this polarization. Note that all of the results are applicable also for the TM_z polarization transformed by the aforementioned simple duality.

2.1. Full-Wave Solution

Following [41–43], we solve the scattering coefficients for a TE_z polarized plane wave that is incident on an RA cylinder with radius ρ_c. The incoming time-harmonic magnetic field with unit amplitude, $H_{0z} = 1$, is given as:

$$\begin{aligned} H_{z,\text{inc}} = e^{-jk_0 x} = e^{-jk_0 \rho \cos(\varphi)} &= \sum_{n=-\infty}^{\infty} (-j)^n J_n(k_0\rho) e^{jn\varphi} \\ &= J_0(k_0\rho) + 2\sum_{n=1}^{\infty} (-j)^n J_n(k_0\rho)\cos(n\varphi), \quad \rho > \rho_c \end{aligned} \tag{8}$$

We write the scattered magnetic field as:

$$H_{z,\text{scat}} = -a_0 H_n^{(2)}(k_0\rho) - 2\sum_{n=-1}^{\infty} a_n (-j)^n H_n^{(2)}(k_0\rho)\cos(n\varphi), \quad \rho > \rho_c \tag{9}$$

where the negative sign follows from the notation of van de Hulst [9] and Bohren and Huffman [10]. Inside the RA cylinder, the magnetic field is:

$$H_{z,\text{in}} = b_0 J_0(k_{\text{in}}\rho) + 2\sum_{n=1}^{\infty} b_n (-j)^n J_{n\gamma}(k_{\text{in}}\rho)\cos(n\varphi), \quad \rho < \rho_c \tag{10}$$

where $\gamma = \sqrt{\varepsilon_\varphi/\varepsilon_\rho}$ and $k_{\text{in}} = \sqrt{\varepsilon_\varphi}\sqrt{\mu_z}k_0$.

The tangential components of the corresponding electric field are:

$$E_{\varphi,\text{inc}} = \frac{jk_0}{\omega\varepsilon_0}\left[J_0'(k_0\rho) + 2\sum_{n=1}^{\infty}(-j)^n J_n'(k_0\rho)\cos(n\varphi)\right], \quad \rho > \rho_c \tag{11}$$

$$E_{\varphi,\text{scat}} = -\frac{jk_0}{\omega\varepsilon_0}\left[a_0 H_0^{(2)\prime}(k_0\rho) + 2\sum_{n=1}^{\infty} a_n(-j)^n H_n^{(2)\prime}(k_0\rho)\cos(n\varphi)\right], \quad \rho > \rho_c \tag{12}$$

$$E_{\varphi,\text{in}} = \frac{jk_{\text{in}}}{\omega\varepsilon_0\varepsilon_\varphi}\left[b_0 J_0'(k_{\text{in}}\rho) + 2\sum_{n=1}^{\infty} b_n(-j)^n J_{n\gamma}'(k_{\text{in}}\rho)\cos(n\varphi)\right], \quad \rho < \rho_c \tag{13}$$

and the continuity of the tangential fields:

$$H_{z,\text{inc}} + H_{z,\text{scat}} = H_{z,\text{in}}$$
$$E_{\varphi,\text{inc}} + E_{\varphi,\text{scat}} = E_{\varphi,\text{in}}$$

at $\rho = \rho_c$ yields for the coefficients:

$$a_n = \frac{\sqrt{\mu_z}J_n(x)J_{n\gamma}'(mx) - \sqrt{\varepsilon_\varphi}J_{n\gamma}(mx)J_n'(x)}{\sqrt{\mu_z}H_n^{(2)}(x)J_{n\gamma}'(mx) - \sqrt{\varepsilon_\varphi}J_{n\gamma}(mx)H_n^{(2)\prime}(x)} \tag{14}$$

$$b_n = \frac{\sqrt{\varepsilon_\varphi}H_n^{(2)}(x)J_n'(x) - \sqrt{\varepsilon_\varphi}J_n(x)H_n^{(2)\prime}(x)}{\sqrt{\mu_z}H_n^{(2)}(x)J_{n\gamma}'(mx) - \sqrt{\varepsilon_\varphi}J_{n\gamma}(mx)H_n^{(2)\prime}(x)} \tag{15}$$

where $m = \sqrt{\mu_z}\sqrt{\varepsilon_\varphi}$ and $x = k_0\rho_c$ is the size parameter of the cylinder. Note that, in the case of an isotropic non-magnetic cylinder, the scattering coefficients a_n reduce to the ones of [9] and [10], but have an opposite sign compared with the ones obtained in [42] and [43]. Hence, the extinction, scattering and absorption efficiencies Q_{ext}, Q_{scat} and Q_{abs}, respectively, are obtained from the Equation (14) as [10]:

$$Q_{\text{ext}} = \frac{2}{x}\,\text{Re}\left\{a_0 + 2\sum_{n=1}^{\infty} a_n\right\} \tag{16}$$

$$Q_{\text{scat}} = \frac{2}{x}\left(|a_0|^2 + 2\sum_{n=1}^{\infty}|a_n|^2\right) \tag{17}$$

$$Q_{\text{abs}} = Q_{\text{ext}} - Q_{\text{scat}} \tag{18}$$

Based on the aforementioned duality of electromagnetic fields Equation (7), the scattering coefficients for TM_z polarization are given as:

$$a_n^{\text{TM}} = \frac{\sqrt{\varepsilon_z}J_n(x)J_{n\tau}'(\ell x) - \sqrt{\mu_\varphi}J_{n\tau}(\ell x)J_n'(x)}{\sqrt{\varepsilon_z}H_n^{(2)}(x)J_{n\tau}'(\ell x) - \sqrt{\mu_\varphi}J_{n\tau}(\ell x)H_n^{(2)\prime}(x)} \tag{19}$$

where $\tau = \sqrt{\mu_\varphi/\mu_\rho}$ and $\ell = \sqrt{\varepsilon_z}\sqrt{\mu_\varphi}$. Equations (16)–(18) are directly applicable for Equation (19) as well.

2.2. Asymptotes of the Scattering Coefficients

The first magnetic and electric TE$_z$ resonances of the cylinder are revealed by the scattering coefficients:

$$a_0 = \frac{\sqrt{\mu_z}J_0(x)J_0'(mx) - \sqrt{\varepsilon_\varphi}J_0(mx)J_0'(x)}{\sqrt{\mu_z}H_0^{(2)}(x)J_0'(mx) - \sqrt{\varepsilon_\varphi}J_0(mx)H_0^{(2)\prime}(x)} \tag{20}$$

and:

$$a_1 = \frac{\sqrt{\mu_z}J_1(x)J_\gamma'(mx) - \sqrt{\varepsilon_\varphi}J_\gamma(mx)J_1'(x)}{\sqrt{\mu_z}H_1^{(2)}(x)J_\gamma'(mx) - \sqrt{\varepsilon_\varphi}J_\gamma(mx)H_1^{(2)\prime}(x)} \tag{21}$$

respectively. Note that whereas a_0 is only a function of ε_φ and μ_z, the coefficient a_1 also depends on ε_ρ in a rather indirect way through $\gamma = \sqrt{\varepsilon_\varphi/\varepsilon_\rho}$. At the long-wavelength limit, where $x \ll 1$, the Equations (20) and (21) can be approximated by asymptotic forms, and the connection between the material parameters and the scattering coefficients becomes much simpler. Applying the following limiting forms of the small-argument Bessel and Hankel functions [10,43]:

$$J_\nu(x) \approx \frac{x^\nu}{2^\nu\Gamma(\nu+1)} \tag{22}$$

$$J_0'(x) \approx -\frac{x}{2} \tag{23}$$

$$H_0^{(2)}(x) \approx -j\frac{2}{\pi}\ln\left(\frac{x}{2}\right) \tag{24}$$

$$H_1^{(2)}(x) \approx j\frac{2}{\pi x} \tag{25}$$

we obtain:

$$a_0 \approx j\frac{\pi}{4}(\mu_z - 1)x^2 \tag{26}$$

$$a_1 \approx j\frac{\pi}{4}\frac{\sqrt{\varepsilon_\rho}\sqrt{\varepsilon_\varphi} - 1}{\sqrt{\varepsilon_\rho}\sqrt{\varepsilon_\varphi} + 1}x^2 \tag{27}$$

In other words, for cylinders small enough, the first coefficient a_0 depends only on permeability μ_z and the second one a_1 only on permittivities ε_ρ and ε_φ.

3. Homogenization Approach for RA Cylinders

The homogenization procedure that we consider for RA cylinders consists of two different levels (see Figure 1). First, we find the effective isotropic parameters for a single cylinder. We start from the static limit and then expand the approach into electrodynamics using the asymptotes of the Mie scattering coefficients. Finally, we consider a composite medium consisting of an array of RA cylinders, whose effective material parameters are estimated using the Maxwell Garnett mixing rule. We further stress that we only consider the TE$_z$ polarization, where the electric field is perpendicular and the magnetic field parallel to the axis of the cylinder. Therefore, the obtained effective permittivities always refer to the components transverse to the cylinder axis, and the effective permeabilities are the z-components that are parallel to the cylinder.

3.1. Homogenization of an Individual Cylinder

The coefficient a_1 in Equation (27) can also be seen in the form:

$$a_1 \approx j\frac{\pi}{8}\alpha x^2 \tag{28}$$

in agreement with [31,32], where:

$$\alpha = 2\frac{\sqrt{\varepsilon_\rho}\sqrt{\varepsilon_\varphi}-1}{\sqrt{\varepsilon_\rho}\sqrt{\varepsilon_\varphi}+1} = 2\frac{\varepsilon_{\text{c,stat}}-1}{\varepsilon_{\text{c,stat}}+1} \tag{29}$$

is the normalized quasi-static polarizability of the RA cylinder. The static effective permittivity of the cylinder:

$$\varepsilon_{\text{c,stat}} = \sqrt{\varepsilon_\rho}\sqrt{\varepsilon_\varphi} \tag{30}$$

is the geometric average of the RA permittivity components [40,42,43]. This means that from the outside, the anisotropic cylinder is observed effectively isotropic. In the static limit, the observed permeability is naturally just $\mu_{\text{c,stat}} = \mu_z$.

The next step is to replace the original material parameters ε_ρ, ε_φ and μ_z in Equations (26) and (27) by frequency-dependent dispersive effective parameters $\varepsilon_{\text{c}}(x)$ and $\mu_c(x)$ and assume that within the considered range of x, the cylinder is electrically small enough, such that these expressions correspond to the exact values of a_0 and a_1 computed using Equations (20) and (21). That is:

$$a_0 \approx j\frac{\pi}{4}(\mu_c(x)-1)x^2 \tag{31}$$

$$a_1 \approx j\frac{\pi}{4}\frac{\varepsilon_{\text{c}}(x)-1}{\varepsilon_{\text{c}}(x)+1}x^2 \tag{32}$$

from which we get approximate formulas for the frequency-dependent effective parameters ε_{c} and μ_c of an individual RA cylinder as:

$$\varepsilon_{\text{c}}(x) \approx \frac{\pi x^2 - j4a_1}{\pi x^2 + j4a_1} \tag{33}$$

$$\mu_c(x) \approx 1 - j\frac{4a_0}{\pi x^2} \tag{34}$$

If the aim is to make the effective permittivity and permeability of a single cylinder be equal for a certain size parameter x, $\varepsilon_{\text{c}}(x) = \mu_c(x)$, the scattering coefficients must satisfy:

$$a_0 = \frac{2a_1\pi x^2}{\pi x^2 + j4a_1} \tag{35}$$

3.2. Homogenization of Composite Media Consisting of RA Cylinders

Moreover, the effective parameters for a lattice of cylinders can be estimated. Assume the cylinders are embedded in a background with $\varepsilon_{\text{b}} = \mu_{\text{b}} = 1$. Provided the cylinders remain electrically small and the area fraction $p = \pi\rho_c^2/d^2$ is small enough (see Figure 1b), the effective permittivity ε_{eff} can be approximated using the Maxwell Garnett mixing formula [49] as:

$$\varepsilon_{\text{eff}} = 1 + 2p\frac{\varepsilon_{\text{c}}-1}{\varepsilon_{\text{c}}+1-p(\varepsilon_{\text{c}}-1)} = 1 - j\frac{8pa_1}{\pi x^2 + j4pa_1} \tag{36}$$

As the magnetic field is parallel to the cylinder axes, the effective permeability μ_{eff} is just the average over the cross-sectional area.

$$\mu_{\text{eff}} = p\mu_c + (1-p) = 1 - j\frac{4pa_0}{\pi x^2} \tag{37}$$

If we want the effective permittivity and permeability of the lattice of cylinders to be equal, $\varepsilon_{\text{eff}}(x) = \mu_{\text{eff}}(x)$, the coefficients must satisfy:

$$a_0 = \frac{2a_1\pi x^2}{\pi x^2 + j4pa_1} \tag{38}$$

Note the surprisingly small difference between Equations (35) and (38).

However, considering many metamaterial applications, it is usually important to obtain the certain given values for the real parts of the material parameters. If we rewrite the expressions (33) and (34) as $\varepsilon_{\text{c}} = \varepsilon'_{\text{c}} - j\varepsilon''_{\text{c}}$ and $\mu_c = \mu'_c - j\mu''_c$, with $a_0 = a'_0 + ja''_0$ and $a_1 = a'_1 + ja''_1$, we obtain:

$$\varepsilon_{\text{c}} \approx \frac{\pi^2x^4 - 16(a_1'^2 + a_1''^2)}{(\pi x^2 - 4a_1'')^2 + 16a_1'^2} - j\frac{8a_1'\pi x^2}{(\pi x^2 - 4a_1'')^2 + 16a_1'^2} \tag{39}$$

$$\mu_c \approx 1 + \frac{4a_0''}{\pi x^2} - j\frac{4a_0'}{\pi x^2} \tag{40}$$

for a single cylinder, and:

$$\varepsilon_{\text{eff}} \approx 1 + \frac{8pa_1''(\pi x^2 - 4pa_1'') - 32p^2a_1'^2}{(\pi x^2 - 4pa_1'')^2 + 16p^2a_1'^2} - j\frac{8pa_1'(\pi x^2 - 4pa_1'') + 32p^2a_1'a_1''}{(\pi x^2 - 4pa_1'')^2 + 16p^2a_1'^2} \tag{41}$$

$$\mu_{\text{eff}} \approx 1 + \frac{4pa_0''}{\pi x^2} - j\frac{4pa_0'}{\pi x^2} \tag{42}$$

for the lattice of cylinders.

Let us assume the original material parameters ε_ρ, ε_φ and μ_z are purely real, so that the coefficients can be conveniently written as:

$$a_n = \frac{U_n}{U_n - jV_n} = \frac{U_n^2}{U_n^2 + V_n^2} + j\frac{U_nV_n}{U_n^2 + V_n^2} = a'_n + ja''_n \tag{43}$$

where:

$$U_n = \sqrt{\mu_z}J_n(x)J'_{n\gamma}(mx) - \sqrt{\varepsilon_\varphi}J_{n\gamma}(mx)J'_m(x) \tag{44}$$

$$V_n = \sqrt{\mu_z}Y_n(x)J'_{n\gamma}(mx) - \sqrt{\varepsilon_\varphi}J_{n\gamma}(mx)Y'_n(x) \tag{45}$$

are real-valued. In this case, Equations (41) and (42) with (43) provide us a design rule to fix the real parts of the effective material parameters by adjusting the original RA parameters ε_ρ, ε_φ and μ_z for a chosen cylinder size parameter x and area fraction p. For μ'_{eff}, we obtain:

$$\mu'_{\text{eff}}(\varepsilon_\varphi, \mu_z, x, p) = 1 + \frac{4pU_0V_0}{\pi x^2(U_0^2 + V_0^2)} \tag{46}$$

For $\varepsilon'_{\text{eff}}$, the equation becomes slightly more complicated as:

$$\varepsilon'_{\text{eff}}(\varepsilon_\rho, \varepsilon_\varphi, \mu_z, x, p) = \frac{\pi^2x^4(U_1^2 + V_1^2)^2 - 16p^2(U_1^2V_1^2 + U_1^4)}{\pi^2x^4(U_1^2 + V_1^2)^2 - 8p\pi x^2(U_1^3V_1 + U_1V_1^3) + 16p^2(U_1^2V_1^2 + U_1^4)} \tag{47}$$

Herein, our approach to find the suitable parameters is to first fix the desired values of $\varepsilon'_{\text{eff}}$ and μ'_{eff}, the corresponding size parameter x and the lattice filling fraction p. Note that $\varepsilon'_{\text{eff}}$ does not necessarily have to equal μ'_{eff}. We could also choose different size parameters x for $\varepsilon'_{\text{eff}}$ and μ'_{eff}. This would mean that the desired values for $\varepsilon'_{\text{eff}}$ and μ'_{eff} are obtained at different frequencies, as the physical size of the cylinder must still remain the same. Then, either μ_z or ε_φ is fixed, and the other one is solved from Equation (46). Finally, the remaining parameter ε_ρ can be solved using Equation (47).

3.3. Artificial Magnetism from All-Dielectric RA Cylinders

It is possible to create a magnetic resonance using purely dielectric RA cylinders just by setting ε_φ large enough. If this resonance is strong enough, even negative values of μ'_{eff} are achievable. Let us consider a case where the real part of the effective permeability of a lattice of all-dielectric RA cylinders would be resonant, such that $\mu'_{\text{eff}} = 0$ for a certain value of the cylinder size parameter x. This parameter should be chosen, such that the unit cells can be assumed small enough to ensure that the lattice is still homogenizable. If the area fraction is chosen $p = 0.2$, which should be large enough considering the effect of the individual cylinders in the effective Equations (36) and (37), but small enough to retain the coupling between adjacent cylinders close to negligible to ensure the accuracy of the coefficients a_n and the validity of Maxwell Garnett mixing rule. With the choice $x = 0.15$, the lattice period corresponds to $d \approx \lambda/10.6$ (see Figure 1b), which is assumed adequate in the following examples.

With these given parameters, the numerical solution of Equation (46) gives the required tangential permittivity component $\varepsilon_\varphi \approx 253$. As the solution is based on the scattering coefficient a_0, it does not depend at all on the radial permittivity ε_ρ, which can be chosen freely. Choosing ε_ρ small enough, the electric resonance of a_1 occurs only at a much higher frequency, and in the vicinity of $x = 0.15$, the obtained ε_{eff} remains close to the Maxwell Garnett estimate Equation (36), where ε_{c} is given by the static value $\varepsilon_{\text{c}} = \sqrt{\varepsilon_\rho}\sqrt{\varepsilon_\varphi}$. For example, choosing $\varepsilon_\rho = 1$ gives $\varepsilon'_{\text{eff}} \approx 1.43$. We can even make the lattice electrically transparent by choosing $\varepsilon_\rho = \varepsilon_\varphi^{-1}$, as found in [40]. Figure 2 presents the obtained μ_{eff} and ε_{eff} using the aforementioned values $\varepsilon_\rho = 1$, $\varepsilon_\varphi = 253$, $\mu_z = 1$, $p = 0.2$. The effective permeability shows a Lorentz-type resonance crossing the zero at $x = 0.15$, whereas within the plotted range, permittivity remains close to $\varepsilon'_{\text{eff}} \approx 1.43$ without noticeable dispersion.

3.4. Double-Negative Response from Magnetodielectric RA Cylinders

Let us then consider the possibility of having both $\varepsilon'_{\text{eff}}$ and μ'_{eff} negative simultaneously. Especially, we focus on the highly desirable case $\varepsilon_{\text{eff}} = \mu_{\text{eff}} = -1$. Let us again choose $p = 0.2$ and the condition $\varepsilon'_{\text{eff}} = \mu'_{\text{eff}} = -1$ to occur at $x = 0.15$. Different RA configurations are presented in Figure 3. It is mathematically possible to solve the required permittivity components to satisfy this condition using only non-magnetic cylinders, choosing $\mu_z = 1$. However, the required permittivity values are not very realistic. The resonance of μ'_{eff} again depends only on ε_φ, which can be found numerically from Equation (46) as $\varepsilon_\varphi \approx 271$. The electric resonance must then be adjusted by ε_ρ, which, however, affects the coefficient a_1 Equation (21) only very weakly via the non-integer order $\gamma = \sqrt{\varepsilon_\varphi/\varepsilon_\rho}$ of the Bessel functions. Thus, the required ε_ρ, obtained from Equation (47),

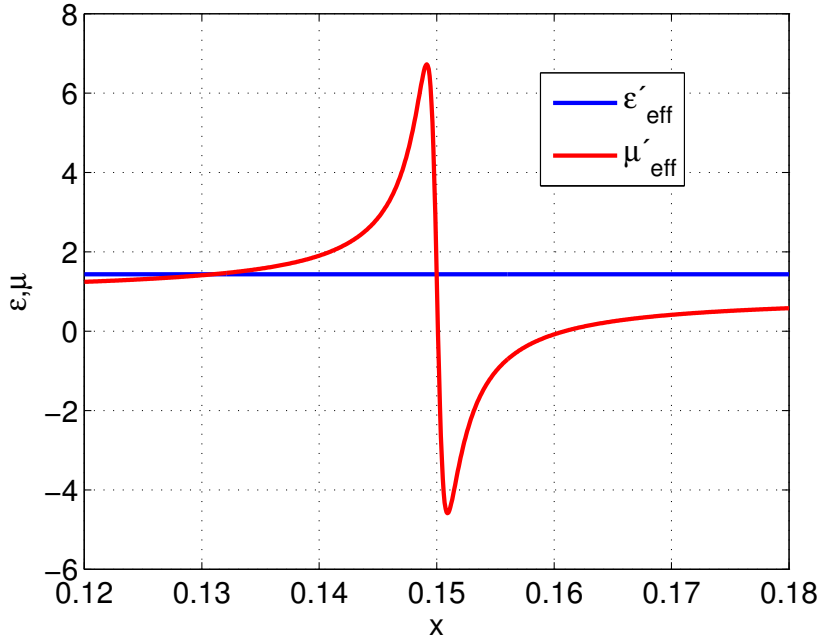

Figure 2. Effective parameters μ'_{eff} and $\varepsilon'_{\text{eff}}$ of a lattice of all-dielectric RA cylinders with $\varepsilon_\rho = 1$, $\varepsilon_\varphi = 253$ and $\mu_z = 1$ with area fraction $p = 0.2$. The lattice exhibits artificial magnetism, and even negative values of μ'_{eff} are achieved.

must be gigantic, in this case $\varepsilon_\rho \approx 120,200$. Moreover, the resonance of $\varepsilon'_{\text{eff}}$ is unpractically narrow (see Figure 3a).

To overcome this problem, we must allow the cylinder to have $\mu_z \neq 1$. For example, the required permittivities become $\varepsilon_\rho \approx 1440$ and $\varepsilon_\varphi \approx 63.7$ for $\mu_z = 5$ (see Figure 3b), $\varepsilon_\rho \approx 270$ and $\varepsilon_\varphi \approx 36.6$ for $\mu_z = 10$ (see Figure 3c), $\varepsilon_\rho \approx 61.4$ and $\varepsilon_\varphi \approx 21.6$ for $\mu_z = 20$ (see Figure 3d), $\varepsilon_\rho \approx 3.38$ and $\varepsilon_\varphi \approx 5.80$ for $\mu_z = 100$ (see Figure 3e) and $\varepsilon_\rho \approx 1.06$ and $\varepsilon_\varphi \approx 3.07$ for $\mu_z = 200$ (see Figure 3f). From these results, we see that μ_z is the most effective parameter considering the scattering coefficients, which is obvious, since the incoming magnetic field H_z is parallel to the (infinitely long) cylinders. By choosing a larger μ_z, the required permittivity components respectively become smaller. Large μ_z shifts the resonance of μ'_{eff} into a smaller frequency, making the resonance also broader. The resonance of $\varepsilon'_{\text{eff}}$ still remains quite narrow, which means that by the condition $\varepsilon'_{\text{eff}} = \mu'_{\text{eff}} = -1$, the actual resonances are shifted further apart, which only makes the design easier with more moderate permittivity values.

Moreover, we note that with small μ_z, the radial component ε_ρ must be larger than the tangential one ε_φ, but with increasing μ_z, this inequality flips around. This means that in between, there is a μ_z value, for which $\varepsilon_\rho \approx \varepsilon_\varphi$. That is, the sought condition $\varepsilon'_{\text{eff}} = \mu'_{\text{eff}} = -1$ can also be achieved using an isotropic magnetodielectric cylinder. It can be numerically solved that the condition is satisfied with $\varepsilon_\rho \approx \varepsilon_\varphi \approx 9.94$ and $\mu_z \approx 53.6$.

3.5. Effects of Different Design Parameters

We have studied the effective material parameters $\varepsilon'_{\text{eff}}$ and μ'_{eff} of a lattice of RA cylinders as functions of initial RA material parameters ε_ρ, ε_φ, μ_z, lattice area fraction p and cylinder size parameters x. As seen

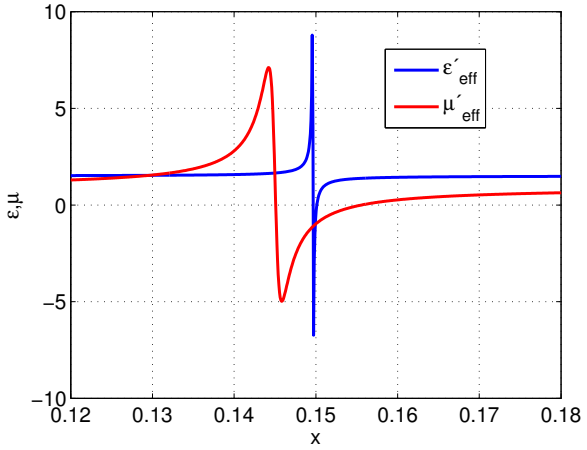

(a) $\varepsilon_\rho \approx 120200$, $\varepsilon_\varphi \approx 271$, $\mu_z = 1$

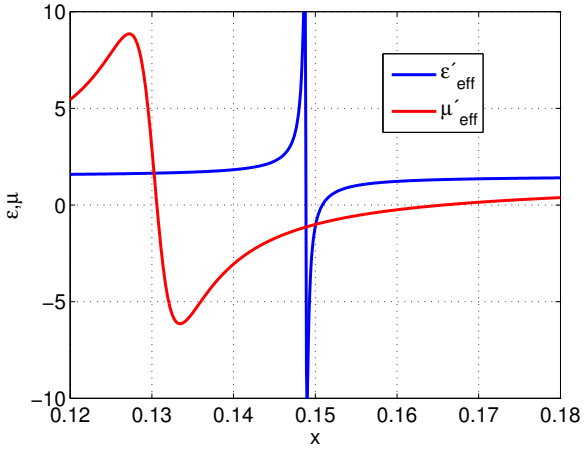

(b) $\varepsilon_\rho \approx 1440$, $\varepsilon_\varphi \approx 63.7$, $\mu_z = 5$

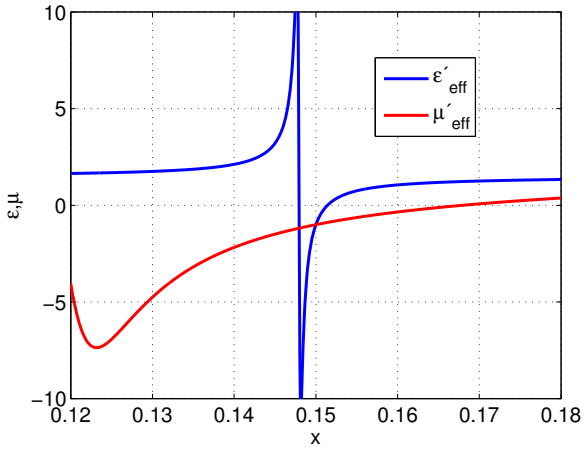

(c) $\varepsilon_\rho \approx 270$, $\varepsilon_\varphi \approx 36.6$, $\mu_z = 10$

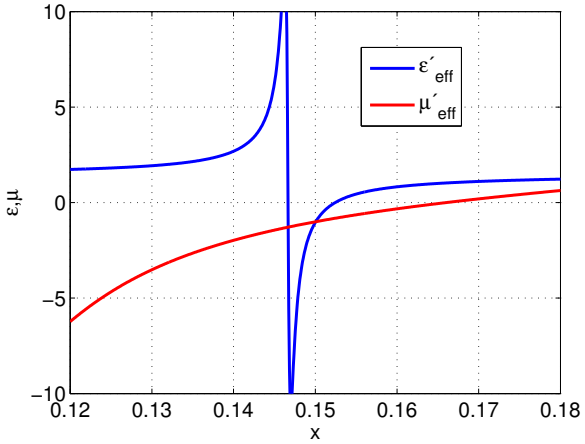

(d) $\varepsilon_\rho \approx 61.4$, $\varepsilon_\varphi \approx 21.6$, $\mu_z = 20$

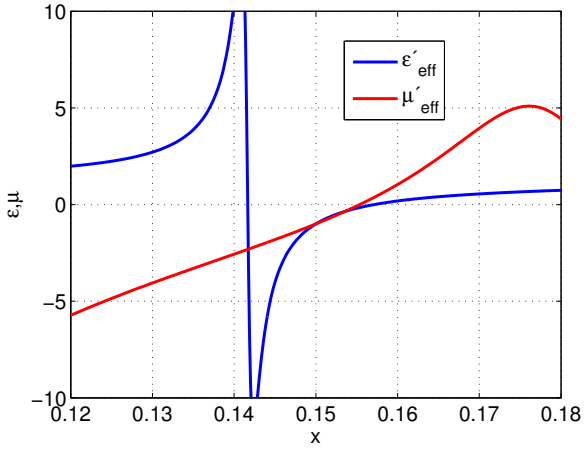

(e) $\varepsilon_\rho \approx 3.38$, $\varepsilon_\varphi \approx 5.80$, $\mu_z = 100$

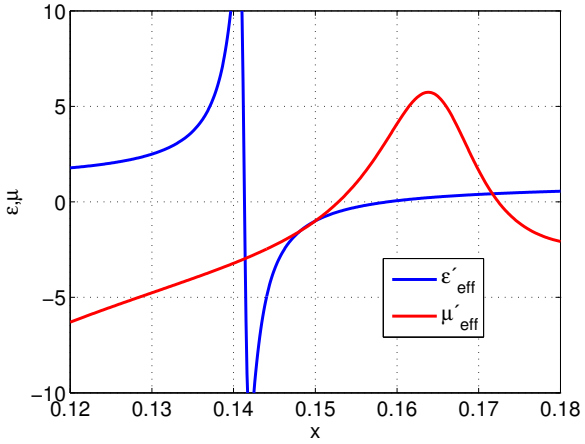

(f) $\varepsilon_\rho \approx 1.06$, $\varepsilon_\varphi \approx 3.07$, $\mu_z = 200$

Figure 3. Effective parameters μ'_{eff} and $\varepsilon'_{\text{eff}}$ of a lattice of magnetodielectric RA cylinders with area fraction $p = 0.2$. All configurations 3a–3f yield $\varepsilon'_{\text{eff}} = \mu'_{\text{eff}} = -1$ at $x = 0.15$.

from the presented results, it is relatively easy to tune the effective permeability μ'_{eff} of the composite consisting of RA cylinders. It is even possible to have negative permeability from purely dielectric cylinders with only ε_φ large enough, as seen in Figure 2. Moreover, allowing $\mu_z \neq 1$, permeability μ'_{eff} can be effectively tuned by parameters μ_z and ε_φ, whereas it is independent of radial permittivity ε_ρ. The effective permittivity $\varepsilon'_{\text{eff}}$, instead, depends on all three parameters of the RA cylinders. Considering achieving the double-negative response using small μ_z, the required ε_ρ has to be respectively gigantic. Therefore, allowing μ_z to be large, the desired magnetic and electric resonances can be tuned with more moderate permittivity values.

The parameter x must be chosen small enough to ensure that the effective medium can be considered homogeneous. This would mean that the lattice constant d should be at least of the order of $\lambda/10$ or preferably even smaller. Shrinking x means bringing the cylinder resonances into lower frequencies, which respectively requires increasing the material parameter values.

The lattice filling fraction p should also be kept small for two reasons. Firstly, the scattering coefficients Equation (14) are derived for a single cylinder surrounded by free space. The cylinders in the lattice must therefore be located wide enough apart to minimize the coupling between each other. Secondly, it is known that the Maxwell Garnett mixing rule is only applicable for small fractions of inclusions. On the other hand, making p larger helps to make the unit cell size electrically smaller, since $d = \rho_c\sqrt{\pi/p}$ (see Figure 1b). As seen from Equation (42), the value of p only affects the amplitude of μ'_{eff}, but for $\varepsilon'_{\text{eff}}$ (see Equation (41)), larger p both increases the amplitude and shifts the resonance into a smaller frequency.

3.6. Omittance of Losses

A very important factor that we have neglected in the analysis above is the effect of material losses. This is due to the simplicity of the analysis. Assuming purely real constituent material parameters enables the simple division of scattering coefficients a_n into their real and imaginary parts, as shown in Equation (43). Complex permittivity values also make the orders of Bessel functions $J_{n\gamma}(x)$ complex, which makes their numerical evaluation more complicated. Therefore, we leave the study of material losses as an objective for future research and introduce the current analysis of the lossless case as a first step towards understanding and evaluating the merits of the proposed structure.

The coefficients Equation (14) are complex numbers, and hence, the obtained ε_{eff} Equations (41) and μ_{eff} (42) are complex-valued. Considering the material parameters, the principle of causality also states that a resonant real part requires a resonant imaginary part. In this particular case of resonant magnetodielectric inclusions, the effective parameters follow the Lorentz dispersion model. However, the imaginary parts are only significant in the vicinity of the resonances, and in this article, we have only considered and presented the real parts. The imaginary parts of the effective parameters ε_{eff} and μ_{eff} must naturally arise from the losses of the intrinsic material parameters ε_ρ, ε_φ and μ_z. Therefore, the presented model for tuning the real parts of the effective medium should be seen as an approximation in the case of negligibly small material losses.

Considering the case in Figure 3 of achieving the condition $\varepsilon'_{\text{eff}} = \mu'_{\text{eff}} = -1$ that is required for superlensing, the losses are especially detrimental [50–52]. Therefore, the two last configurations (see

Figure 3e and 3f) are the most suitable, since the actual resonances occur on lower frequencies and around the point where $\varepsilon'_{\text{eff}} = \mu'_{\text{eff}} = -1$ the dispersion of the curves is more moderate. This also implies that the corresponding imaginary parts $\varepsilon''_{\text{eff}}$ and μ''_{eff} have already been significantly attenuated from their maximum resonant values.

4. Conclusions

In this paper, we theoretically studied constructing an effective medium using an array of RA cylinders under TE_z excitation. We derived approximative analytical models for material parameters $\varepsilon'_{\text{eff}}$ and μ'_{eff} as functions of five design parameters, namely radial and tangential permittivities and the axial permeability of the individual cylinders, ε_ρ, ε_φ and μ_z, respectively, area fraction p of the cylinders in the lattice and the fixed cylinder size parameter $x = k_0\rho_c$, which depends on the frequency and the cylinder radius.

We introduced a homogenization method for RA cylinders based on their Mie scattering coefficients and showed how the anisotropy provides additional parameters for tuning the effective response without making the analysis much more complex. We also discussed two possible applications. First, we studied the magnetic response of an all-dielectric cylinder. It is known that even isotropic dielectric cylinders support magnetic Mie resonances and can be applied in constructing mu-negative (MNG) materials. Our analysis revealed that the lowest order magnetic resonance, however, only depends on the tangential permittivity ε_φ of the cylinder. For an RA cylinder, the radial component ε_ρ remains a free parameter and can be used in tuning also its electric response.

Second, we showed that all-dielectric RA cylinders can also manifest a double-negative response. Especially, we considered obtaining negative refractive index $n = -1$ at a given frequency. However, for the chosen TE_z polarization, the required permittivity components had to be enormous, and the achieved bandwidth was rather narrow. By allowing the cylinder to be also magnetic in the axial direction, $\mu_z > 1$, the DNG condition could be adjusted more effectively and with more moderate permittivity components. The last two example configurations shown in Figure 3e and 3f start to resemble a complementary case of [35], where for TM_z polarization, a double-negative region is theoretically and experimentally found for non-magnetic isotropic rods with very large permittivity. However, in our RA case, allowing the permittivity components $\varepsilon_\rho \neq \varepsilon_\varphi \neq 1$, we have free parameters for (theoretically) tuning the desired DNG value for chosen frequency.

Similar homogenization for spherical particles is considered in several papers based on the seminal work of [14–16] (see also the review articles [7] and [8] and the references therein). The two lowest Mie resonances for a sphere are given by the scattering coefficients a_1 and b_1 [10]. Due to the spherical symmetry, the corresponding expressions for the effective parameters of a mixture of spheres are symmetrical functions with respect to coefficients a_1 and b_1, whereas the asymptotes of these coefficients are symmetrical with respect to the original relative material parameters ε_{s} and μ_{s} of an isotropic magnetodielectric sphere. This means that the condition $\varepsilon_{\text{eff}} = \mu_{\text{eff}}$ for a lattice of magnetodielectric spheres, which follows from $a_1 = b_1$, is easily achieved by choosing $\varepsilon_{\text{r}} = \mu_r$ [19]. This is not the case with cylindrical inclusions. As can be seen, the Equations (26) and (27), (33) and (34) or (36) and (37) do not share a similar form with each other.

A realization that uses cylinders is easier to construct, as they would need to be supported only from their ends, but spherical inclusions always need some supporting background material. Introducing an additional background material often lowers the contrast between the inclusions and the environment, which further dampens the scattering from the inclusions. On the other hand, cylindrical geometry has a different response for two orthogonal polarizations, whereas spheres would construct materials that are polarization independent. Hence, we will continue with similar studies for radially-anisotropic spheres.

In our analysis, we neglected the effect of losses for simplicity and obtained an approximative model that can be seen as a limiting case of vanishingly small losses. Therefore, taking the actual effects of losses into account in future research is crucial. It is also important to study the validity of the homogenization models with respect to increasing inclusion size parameters. Alternatively, it would be interesting to study how radially-anisotropic inclusions behave in the photonic regime.

The benefits of RA inclusions are based on the increased variety of intrinsic material parameter components, whereas their geometry itself may remain canonical. Hence, the mathematical analysis of RA cylinders and spheres is not significantly more complicated in comparison to the isotropic ones. Moreover, RA geometries are rotationally symmetric, and to an outside observer, they even seem effectively isotropic. The actual challenge in RA geometries, which we have not considered herein, is finding the suitable natural materials and developing methods to physically construct, for example, the structures suggested in Figure 1a. However, we see that this is worth pursuing, since RA materials show huge potential considering the development of adjustable dielectric-based broadband and low-loss artificial materials.

Acknowledgments

The work of H. Kettunen was supported by the Academy of Finland projects 260522 and CoE-250215.

Author Contributions

This article is based on long-term collaborative work between the authors. All three authors contributed in setting the research questions and discussing the results. H. Kettunen computed the presented results and prepared the manuscript, which was commented on and improved by H. Wallén and A. Sihvola.

Conflicts of Interest

The authors declare no conflict of interest.

References

1. Engheta, N.; Ziolkowski, R.W. *Metamaterials: Physics and Engineering Explorations*; Wiley-Interscience: Hoboken, NJ, USA, 2006.
2. Veselago, V.G. The electrodynamics of substances with simultaneously negative values of ϵ and μ. *Sov. Phys. Uspekhi* **1968**, *10*, 509–514.
3. Pendry, J.B. Negative refraction makes a perfect lens. *Phys. Rev. Lett.* **2000**, *85*, 3966–3969.

4. Maier, S.A. *Plasmonics: Fundamentals and Applications*; Springer: New York, NY, USA, 2007.
5. Pendry, J.B.; Holden, A.J.; Robbins, D.J.; Stewart, W.J. Magnetism for conductors and enhanced nonlinear phenomena. *IEEE Trans. Microwave Theory Tech.* **1999**, *47*, 2075–2084.
6. O'Brien, S.; Pendry, J.B. Photonic band-gap effects and magnetic activity in dielectric composites. *J. Phys. Condens. Matter* **2002**, *14*, 4035–4044.
7. Zhao, Q.; Zhou, J.; Zhang, F.; Lippens, D. Mie resonance-based dielectric metamaterials. *Mat. Today* **2009**, *12*, 60–69.
8. Ueda, T.; Itoh, T. Mu-negative, double-negative, and composite right/left handed metamaterials based on dielectric resonators. *IEICE Electron. Exp.* **2012**, *9*, 65–80.
9. Van de Hulst, H.C. *Light Scattering by Small Particles*; Dover: New York, NY, USA, 1981.
10. Bohren, C.F.; Huffman, D.R. *Absorption and Scattering of Light by Small Particles*; Wiley: New York, NY, USA, 1998.
11. Monticone, F.; Alù, A. The quest for optical magnetism: From split-ring resonators to plasmonic nanoparticles and nanoclusters. *J. Mater. Chem. C* **2014**, *2*, 9059–9072.
12. Kuznetsov, A.I.; Miroshnichenko, A.E.; Fu, Y.H.; Zhang, J.B.; Luk'yanchuk, B. Magnetic light. *Sci. Rep.* **2012**, *2*, 1–6.
13. Ginn, J.C.; Brener, I.; Peters, D.W.; Wendt, J.R.; Stevens, J.O.; Hines, P.F.; Basilio, L.I.; Warne, L.K.; Ihlefeld, J.F.; Clem, P.G.; *et al*. Realizing optical magnetism from dielectric metamaterials. *Phys. Rev. Lett.* **2012**, *108*, 097402:1–5.
14. Gans, R.; Happel, H. Zur Optik kolloidaler Metallösungen. *Ann. Phys. (Leipzig)* **1909**, *334*, 277–300.
15. Stratton, J.A. The effect of rain and fog on the propagation of very short radio waves. *Proc. IRE* **1930**, *18*, 1064–1074.
16. Lewin, L. The electrical constants of a material loaded with spherical particles. *Proc. Inst. Elec. Eng.* **1947**, *94*, 65–68.
17. Waterman, P.C.; Pedersen, N.E. Electromagnetic scattering by periodic arrays of particles. *J. Appl. Phys.* **1986**, *59*, 2609–2618.
18. Grimes, C.A.; Grimes, D.M. Permeability and permittivity spectra of granular materials. *Phys. Rev. B* **1991**, *43*, 10780–10788.
19. Holloway, C.L.; Kuester, E.F.; Baker-Jarvis, J.; Kabos, P. A double negative (DNG) composite medium composed of magnetodielectric spherical particles embedded in a matrix. *IEEE Trans. Antennas. Propag.* **2003**, *51*, 2596–2603.
20. Wheeler, M.S.; Aitchison, J.S.; Mojahedi, M. Three-dimensional array of dielectric spheres with an isotropic negative permeability at infrared frequencies. *Phys. Rev. B* **2005**, *72*, 193103:1–4.
21. Wheeler, M.S.; Aitchison, J.S.; Mojahedi, M. Coated nonmagnetic spheres with a negative index of refraction at infrared frequencies. *Phys. Rev. B* **2006**, *73*, 045105:1–7.
22. Jylhä, L.; Kolmakov, I.; Maslovski, S.; Tretyakov, S. Modeling of isotropic backward-wave materials composed of resonant spheres. *J. Appl. Phys.* **2006**, *99*, 043102:1–7.
23. Vendik, I.; Vendik, O.; Kolmakov, I.; Odit, M. Modelling of isotropic double negative media for microwave applications. *Opto-Electron. Rev.* **2006**, *14*, 179–186.

24. Chern, R.-L.; Liu, X.X. Effective parameters and quasi-static resonances for periodic arrays of dielectric spheres. *J. Opt. Soc. Am. B* **2010**, *27*, 488–497.
25. Kuester, E.F.; Memić, N.; Shen, S.; Scher, A.; Kim, S.; Kumley, K.; Loui, H. A negative refrective index metamaterial based on a cubic array of layered nonmagnetic spherical particles. *Prog. Electromagn. Res. B* **2011**, *33*, 175–202.
26. Liu, L.Y.; Yang, D.P.; Zhou, Y.M.; Zhou, J. Artificial isotropic magnetism and negative refraction of metamaterial consisting of dielectric spherical shells. *Appl. Phys. A* **2014**, *117*, 747–753.
27. Schuller, J.A.; Zia, R.; Taubner, T.; Brongersma, M.L. Dielectric metamaterials based on electric and magnetic resonances of silicon carbide particles. *Phys. Rev. Lett.* **2007**, *99*, 107401:1–4.
28. Vynck, K.; Felbacq, D.; Centeno, E.; Căbuz, A.I.; Cassagne, D.; Guizal, B. All-Dielectric rod-type metamaterials at optical frequencies. *Phys. Rev. Lett.* **2009**, *102*, 133901:1–4.
29. Chern, R.-L.; Chen, Y.T. Effective parameters for photonic crystals with large dielectric contrast. *Phys. Rev. B* **2009**, *80*, 075118:1–9.
30. Townsend, S.; Zhou, S.; Li, Q. Multiscale metamaterials: a new route to isotropic double-negative behaviour at visible frequencies. *Opt. Express* **2014**, *22*, 21929–21937.
31. Kallos, E.; Chremmos, I.; Yannopapas, V. Resonance properties of optical all-dielectric metamaterials using two-dimensional multipole expansion. *Phys. Rev. B* **2012**, *86*, 245108:1–10.
32. Strickland, D.; Ayón, A.; Alù, A. Dynamic polarizability tensor for circular cylinders. *Phys. Rev. B* **2015**, *91*, 085104:1–10.
33. Dirksen, A.; Arslanagic, S.; Breinbjerg, O. Resonances and dipole moments in dielectric, magnetic and magnetodielectric cylinders – an overview. *Appl. Phys. A* **2011**, *103*, 789–793.
34. Bouchitté, G.; Felbacq, D. Homogenization near resonances and artificial magnetism from dielectrics. *C. R. Acad. Sci. Paris Ser. I* **2004**, *339*, 377–382.
35. Peng, L.; Ran, L.; Chen, H.; Zhang, H.; Kong, J.A.; Grzegorczyk, T.M. Experimental observation of left-handed behavior in an array of standard dielectric resonators. *Phys. Rev. Lett.* **2007**, *98*, 157403:1–4.
36. Valdivia-Valero, F.J.; Nieto-Vesperinas, M. Composites of resonant dielectric rods: A test of their behavior as metamaterial refractive elements. *Photonics Nanostruct.* **2012**, *10*, 423–434.
37. Němec, H.; Kužel, P.; Kadlec, F.; Kadlec, C.; Yahiaoui, R.; Mounaix, P. Tunable terahertz metamaterials with negative permeability. *Phys. Rev. B* **2009**, *79*, 241108(R):1–4.
38. Kang, L.; Lippens, D. Mie resonance based left-handed metamaterial in the visible frequency range. *Phys. Rev. B* **2011**, *83*, 195125:1–6.
39. Yu, X.; Gao, L. Nonlinear dielectric response in partially resonant composites with radial dielectric anisotropy. *Phys. Lett. A* **2006**, *359*, 516–522.
40. Kettunen, H.; Wallén, H.; Sihvola, A. Cloaking and magnifying using radial anisotropy. *J. Appl. Phys.* **2013**, *114*, 044110:1–9.
41. Ni, Y.; Gao, L.; Qiu, C.-W. Achieving invisibility of homogeneous cylindrically anisotropic cylinders. *Plasmonics* **2010**, *5*, 251–258.
42. Jin, Y.W.; Gao, D.L.; Gao, L. Plasmonic resonant light scattering by a cylinder with radial anisotropy. *Prog. Electromagn. Res.* **2010**, *106*, 335–347.

43. Chen, H.L.; Gao, L. Anomalous electromagnetic scattering from radially anisotropic nanowires. *Phys. Rev. A* **2012**, *86*, 033825:1–8.
44. Gao, L.; Fung, T.H.; Yu, K.W.; Qiu, C.W. Electromagnetic transparency by coated spheres with radial anisotropy. *Phys. Rev. E* **2008**, *78*, 046609:1–11.
45. Wallén, H.; Kettunen, H.; Sihvola, A. Anomalous absorption, plasmonic resonances, and invisibility of radially anisotropic spheres. *Radio Sci.* **2015**, *50*, 18–28.
46. Ishii, S.; Inoue, S.-I.; Otomo, A. Electric and magnetic resonances in strongly anisotropic particles. *J. Opt. Soc. Am. B* **2014**, *31*, 218–222.
47. Mangini, F.; Tedeschi, N.; Frezza, F.; Sihvola, A. Homogenization of a multilayer sphere as a radial uniaxial sphere: Features and limits. *J. Electromagnet. Wave.* **2014**, *28*, 916–931.
48. Lindell, I.V. *Methods for Electromagnetic Field Analysis*, 2nd ed.; IEEE: New York, NY, USA, 1995.
49. Sihvola, A. *Electromagnetic Mixing Formulas and Applications*; IEEE: London, UK, 1999.
50. Shen, J.T.; Platzman, P.M. Near field imaging with negative dielectric constant lenses. *Appl. Phys. Lett.* **2002**, *80*, 3286–3288.
51. Smith, D.R.; Schurig, D.; Rosenbluth, M.; Schultz, S.; Ramakrishna, S.A.; Pendry, J.B. Limitations on subdiffraction imaging with a negative refractive index slab. *Appl. Phys. Lett.* **2003**, *82*, 1506–1508.
52. Podolskiy, V.A.; Narimanov, E.E. Near-sighted superlens. *Opt. Lett.* **2005**, *30*, 75–77.

© 2015 by the authors; licensee MDPI, Basel, Switzerland. This article is an open access article distributed under the terms and conditions of the Creative Commons Attribution license (http://creativecommons.org/licenses/by/4.0/).